Available online at www.sciencedirect.com
ScienceDirect
Trans. Nonferrous Met. Soc. China 32(2022) 1994−2002
Transactions of Nonferrous Metals Society of China
www.tnmsc.cn

Deposition of Pd on $Co(OH)_2$ nanoplates in stabilizer-free aqueous phase for catalytic reduction of 4-nitrophenol

Zeng-min TANG[1], Ling ZHANG[1], Jing-jing DU[2], Li-jian XU[1]

1. Hunan Key Laboratory of Biomedical Nanomaterials and Devices, College of Life Sciences and Chemistry, Hunan University of Technology, Zhuzhou 412007, China;
2. College of Packaging and Materials Engineering, Hunan University of Technology, Zhuzhou 412007, China

Received 30 May 2021; accepted 24 January 2022

Abstract: Palladium-supported cobalt hydroxide ($Co(OH)_2$-Pd) nanoplates were fabricated in an aqueous solution and employed as a catalyst for the reduction of 4-nitrophenol. For the preparation of $Co(OH)_2$-Pd, Pd nanoparticles were anchored on the $Co(OH)_2$ nanoplates after the reduction of Na_2PdCl_4 by ascorbic acid in the absence of a stabilizer at room temperature. The observations under transmission and scanning electron microscopy reveal that Pd nanoparticles with a size of 2–5 nm are uniformly dispersed on the surface of the $Co(OH)_2$ nanoplates. In catalytic test, the conversion of 4-nitrophenol to 4-aminophenol is completed within 6 min in the presence of $Co(OH)_2$-Pd(1000) nanoplates with 2.18 at.% Pd, and the corresponding kinetic constant is 0.0089 s^{-1} in the first test. The catalyst retains relatively high activity after several cycles. The results demonstrate that the $Co(OH)_2$-Pd(1000) nanoplates exhibit high catalytic activity toward the reduction of 4-nitrophenol in the presence of $NaBH_4$.
Key words: Pd nanoparticles; $Co(OH)_2$ nanoplates; free stabilizer; catalyst; 4-nitrophenol

1 Introduction

Nitrophenols, including para-, meta-, and ortho-nitrophenol, are a type of hazardous and toxic pollutants found in wastewater originating from industrial and agricultural sources. Para-nitrophenol (4-NP) has been listed as a priority pollutant by the US Environmental Protection Agency because of its high solubility and stability in water [1,2]. Many strategies have been developed for pollutant removal and conversion, such as adsorption, microbial/photocatalytic degradation, and catalytic oxidation/reduction [3−10]. In particular, the conversion of 4-NP to 4-aminophenol (4-AP) over a catalyst in an aqueous solution under mild conditions may be considered as an effective, energy-saving, and green strategy for wastewater treatment [11]. In addition, 4-AP is an important intermediate in the manufacture of analgesic and antipyretic drugs, such as acetanilide, paracetamol, and phenacetin [12]. Therefore, it is important to develop a process for the catalytic hydrogenation of 4-NP to 4-AP.

Among various catalysts, Pd has received considerable attention because of its high catalytic activity for the conversion of 4-NP. In particular, nanosized Pd particles with a large surface area exhibit high catalytic performance toward 4-NP hydrogenation [13]. However, Pd nanoparticles with high surface energy easily undergo aggregation during the process of synthesis and catalysis reactions. The coating of the surface of Pd nanoparticles with a stabilizer can effectively prevent aggregation. However, the presence of such a coating layer blocks the transfer of electrons, leading to a decrease in the catalytic activity [14]. In addition, small Pd nanoparticles are difficult to

Corresponding author: Li-jian XU, Tel: +86-731-22183206, E-mail: xlj235@163.com
DOI: 10.1016/S1003-6326(22)65925-9

separate from the treated solution, resulting in low recyclability [15,16]. Recently, a strategy to immobilize Pd on various carriers (e.g., carbon materials, metal and metal oxides, metal/covalent organic frameworks, silicon materials, and zeolitic imidazolate frameworks) has been considered to be effective because of the recyclability of the composite systems and prevention of aggregation during the treatment of 4-NP [17−23]. LIU et al [24] loaded Pd nanoparticles on 3D-printed hierarchically porous TiO_2 scaffolds, which showed excellent catalytic activity (1063 times higher than that of the Pd/TiO_2-bulk material) and high reusability (no obvious decrease in catalytic activity after 20 cycles). However, the complex fabrication process and high energy input (long synthesis time and high reaction temperature of 900 °C) to synthesize TiO_2 scaffolds severely limit the application and development of such systems. Among various carrier materials, $Co(OH)_2$ is effective because of its excellent electrochemical properties, simple synthesis, and low cost. LONG et al [25] deposited Pt−Au alloy nanoparticles on ultrathin α-$Co(OH)_2$ nanoplates via one-pot synthesis. The prepared Pt−Au/$Co(OH)_2$ nanocomposites exhibited excellent catalytic activity and stability toward the catalytic reduction of 4-NP in the presence of $NaBH_4$. In addition, other metals such as Pt, Pd, and Cu were also anchored on $Co(OH)_2$, and the performance of such composite systems as catalysts was investigated [26−28].

In this work, $Co(OH)_2$-Pd nanoplates were synthesized in the aqueous phase without the use of a stabilizer at room temperature. In the process, the pre-prepared $Co(OH)_2$ nanoplates were employed as support, and ascorbic acid was served as a reducing agent. Small Pd nanoparticles were well dispersed on the surface of $Co(OH)_2$ after the reduction of Na_2PdCl_4 by ascorbic acid in a stabilizer-free aqueous solution. Finally, the catalytic performance of the $Co(OH)_2$−Pd nanoplates toward the reduction of 4-NP was evaluated.

2 Experimental

2.1 Materials

Cobalt chloride hexahydrate ($CoCl_2·6H_2O$, 99%), *n*-octylamine ($C_8H_{19}N$, 98%), ascorbic acid ($C_6H_8O_6$, purity ≥99%), sodium borohydride ($NaBH_4$, 98%), branched polyethyleneimine (BPEI, M_r=60000, 50 wt.% in water), sodium tetrachloropalladate (Na_2PdCl_4, 98%), 4-nitrophenol (4-NP, $C_6H_5NO_3$, 99%), and ethanol (C_2H_5OH, 99.5%) were purchased from Innochem.

2.2 Synthesis of $Co(OH)_2$ nanoplates

Well-dispersed $Co(OH)_2$ nanoplates were fabricated according to a previously reported method [29]. BPEI (60 mg) and $CoCl_2·6H_2O$ (2 mmol) were added to a vial, which was filled with water (8 mL). The vial was then placed in an oil bath with 90 °C and vigorously stirred. Next, octylamine (1 mL) was added to the vial. After 60 min, the vial filled with $Co(OH)_2$ suspension was removed from the oil bath and naturally cooled to room temperature. The pristine $Co(OH)_2$ nanoplates were redispersed in water (10 mL) after washing with ethanol and drying in a vacuum oven.

2.3 Synthesis of $Co(OH)_2$-Pd nanoplates

The Na_2PdCl_4 solution (10 mmol/L) at various volumes (500, 1000, and 1500 μL) was added to an aqueous $Co(OH)_2$ suspension (10 mL) and stirred at room temperature for 2 min. Then, the ascorbic acid solution (0.2 mol/L, 0.5 mL) was injected into the mixed suspension, followed by stirring for 20 min to obtain $Co(OH)_2$-Pd nanoplates which were separated by centrifugation and dried in a vacuum oven at 60 °C for 12 h. The obtained samples are denoted as $Co(OH)_2$-Pd(500), $Co(OH)_2$-Pd(1000), and $Co(OH)_2$-Pd(1500).

2.4 Catalytic activity of $Co(OH)_2$-Pd nanoplates

The reduction of 4-NP was chosen to analyze the catalytic performance of the as-prepared $Co(OH)_2$-Pd nanoplates. The $Co(OH)_2$-Pd nanoplates (3 mg) were first added to a mixture containing 4-NP solution (5 mmol/L, 4.5 mL) and $NaBH_4$ solution (1 mol/L, 0.5 mL). After addition, the mixed suspension was stirred continuously. At a certain time interval, 30 μL of the mixed suspension was injected into a quartz cuvette with 3 mL of water, and the corresponding UV-Vis spectra were recorded.

2.5 Characterization

Scanning electron microscopy (SEM) was conducted on a LEO SUPRA 55 microscope

(Germany, Oberkochen). Powder X-ray diffraction (XRD) analysis was performed on a Rigaku D-MAX/A diffractometer (Japan, Rigaku Corporation) at 35 kV and 35 mA. Transmission electron microscopy (TEM) was carried out on a JEM−2100F microscope. The composition of the samples was analyzed through energy-dispersive X-ray spectroscopy (EDS, INCA, Oxford Company) and X-ray photoelectron spectroscopy (XPS, Thermo Scientific K-Alpha spectrometer). The UV-Vis spectra were recorded using a Jasco UV-Vis spectrophotometer in the range of 250−550 nm.

3 Results and discussion

3.1 Characterization of $Co(OH)_2$ nanoplates

As shown in the SEM images of Figs. 1(a) and (b), most of the samples present hexagonal and round nanoplates. The $Co(OH)_2$ nanoplates exhibit a wide size distribution. The mean size of the plane is (9.70±3.78) μm and the thickness is in the range of 200−400 nm. The XRD pattern shows a strong diffraction peak at 2θ=19.2°, which is assigned to the (001) facet of β-$Co(OH)_2$ (Fig. 1(d), Joint Committee on Powder Diffraction Standards JCPDS file No. 30-0443).

3.2 Characterization of $Co(OH)_2$-Pd nanoplates

The as-prepared $Co(OH)_2$ nanoplates with two-dimensional structures were employed as carriers to fabricate the $Co(OH)_2$-Pd(1000) nanoplates. As shown in Fig. 2(a), the low-resolution image of the sample demonstrates that the morphology of the product does not change during the fabrication process. By further observing the surface of the nanoplates (Figs. 2(b) and (c)), a large number of small nanoparticles are deposited on the surface of the nanoplates. During the synthesis, it is speculated that the Na_2PdCl_4 is first reduced to Pd after the addition of ascorbic acid. Then, active Pd attaches to the surface of $Co(OH)_2$ nanoplates and grows into a nanoparticle in the absence of a stabilizer. However, the characteristic diffraction peak associated with Pd is not observed in the XRD pattern, as shown in Fig. 2(d). This may be due to the low Pd content on the $Co(OH)_2$ nanoplates.

Simultaneously, the hybrid nanoplate samples were analyzed through TEM. The images of Figs. 3(a, b) reveal the presence of large amounts of nanoparticles with a small size (2–5 nm) on the surface of the nanoplates. The TEM image with a high resolution, shown in Fig. 3(c), confirms that

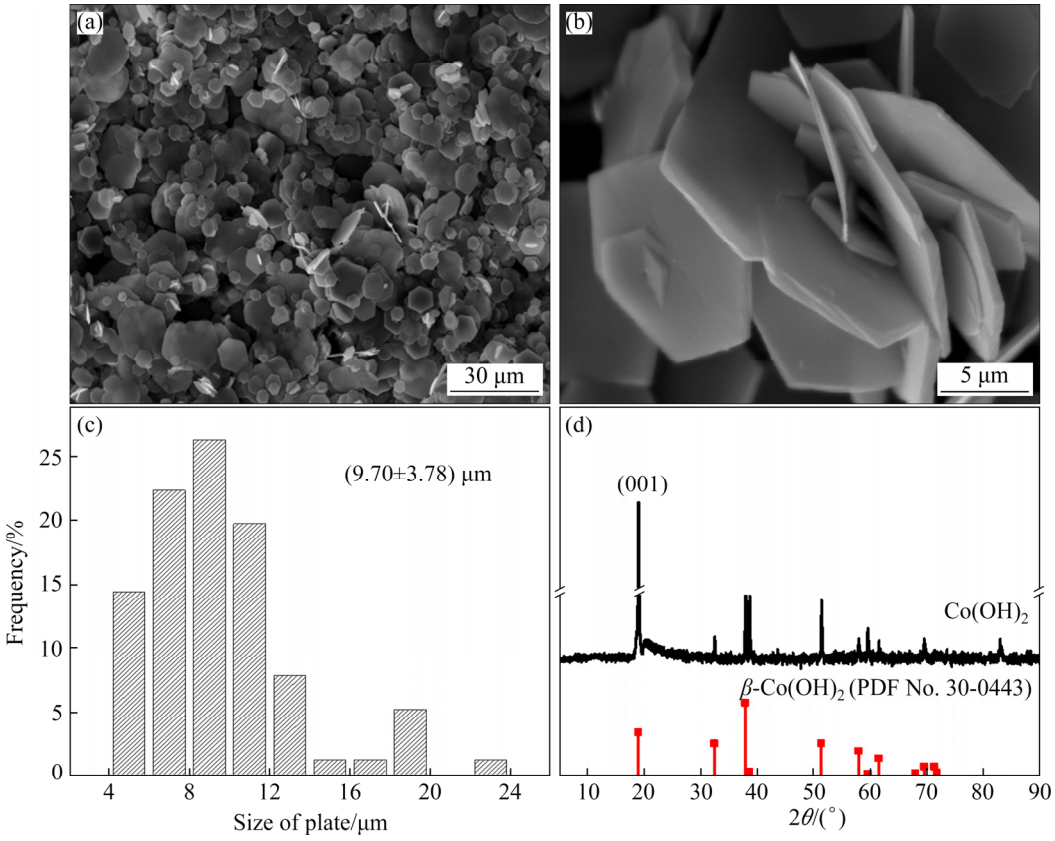

Fig. 1 SEM images (a, b), size distribution (c), and XRD pattern (d) of $Co(OH)_2$ nanoplates

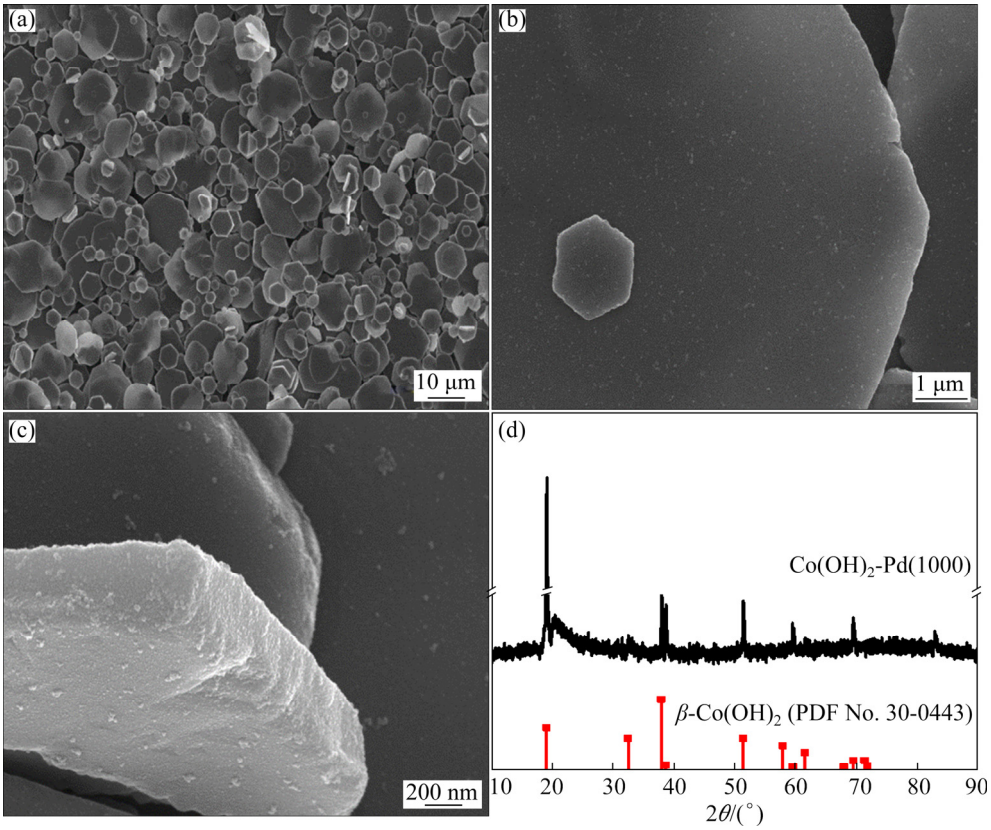

Fig. 2 SEM images (a, b, c) and XRD pattern (d) of $Co(OH)_2$-Pd(1000) nanoplates

the lattice distance of the nanoparticles is approximately 2.2 Å, which corresponds to the (111) facet of Pd. Furthermore, EDS mapping (see Figs. 3(d, e)) clearly shows that Pd is uniformly distributed on the surface of the nanoplates and the molar fraction of Pd is 2.18% (Fig. 3(f)). These results demonstrate that the Pd nanoparticles were formed and were anchored on the surface of the $Co(OH)_2$ nanoplates to form the $Co(OH)_2$-Pd nanoplates.

XPS was conducted to investigate the valence states of Co, O, and Pd atoms in $Co(OH)_2$-Pd(1000). Figure 4(a) shows XPS survey spectra of $Co(OH)_2$-Pd(1000). The Co 2p spectrum shown in Fig. 4(b) consists of $2p_{3/2}$ and $2p_{1/2}$ peaks ascribed to the spin–orbit coupling. The main peaks are located at 779.08 and 794.58 eV, which are assigned to the binding energies of the Co^{2+} oxidation state. Furthermore, the spin-orbit splitting between Co $2p_{1/2}$ and Co $2p_{3/2}$ is approximately 15.5 eV, thereby confirming the presence of Co^{2+} in the form of $Co(OH)_2$ nanoplates. Two satellite peaks at 783.9 and 800.7 eV indicate that Co mainly exists in the Co^{2+} state [30]. The O 1s core-level XPS spectrum is displayed in Fig. 4(c), only the strongest peak at 530.4 eV is observed, which further indicates the existence of $Co(OH)_2$ [31]. In Fig. 4(d), two peaks at 333.48 and 338.68 eV are attributed to $3d_{5/2}$ and $3d_{3/2}$ of Pd (0), respectively. The weak peak at 341.2 eV is assigned to the Pd(II) oxidation state, which may arise because of the incomplete reaction of the Pd precursor [32]. The XPS spectrum further confirms the presence of Pd nanoparticles in the zero-oxidation state. In addition, Pd content (3.14 at.%) measured by XPS is a little higher than that obtained through EDS, which further demonstrates that Pd nanoparticles are coated on the surface of $Co(OH)_2$ to obtain the $Co(OH)_2$-Pd hybrid nanoplates having a core–shell structure.

3.3 Catalytic performance of $Co(OH)_2$-Pd nanoplates

The catalytic performance of the $Co(OH)_2$-Pd nanoplates was estimated for the reduction of 4-NP to 4-AP in the presence of $NaBH_4$. The results are shown in Fig. 5(a). Generally, the aqueous solution of 4-NP in the presence of $NaBH_4$ can be transformed into 4-nitrophenolate ions. These ions exhibit strong absorption at 400 nm and 4-AP exhibits a weak absorption at around 300 nm. In

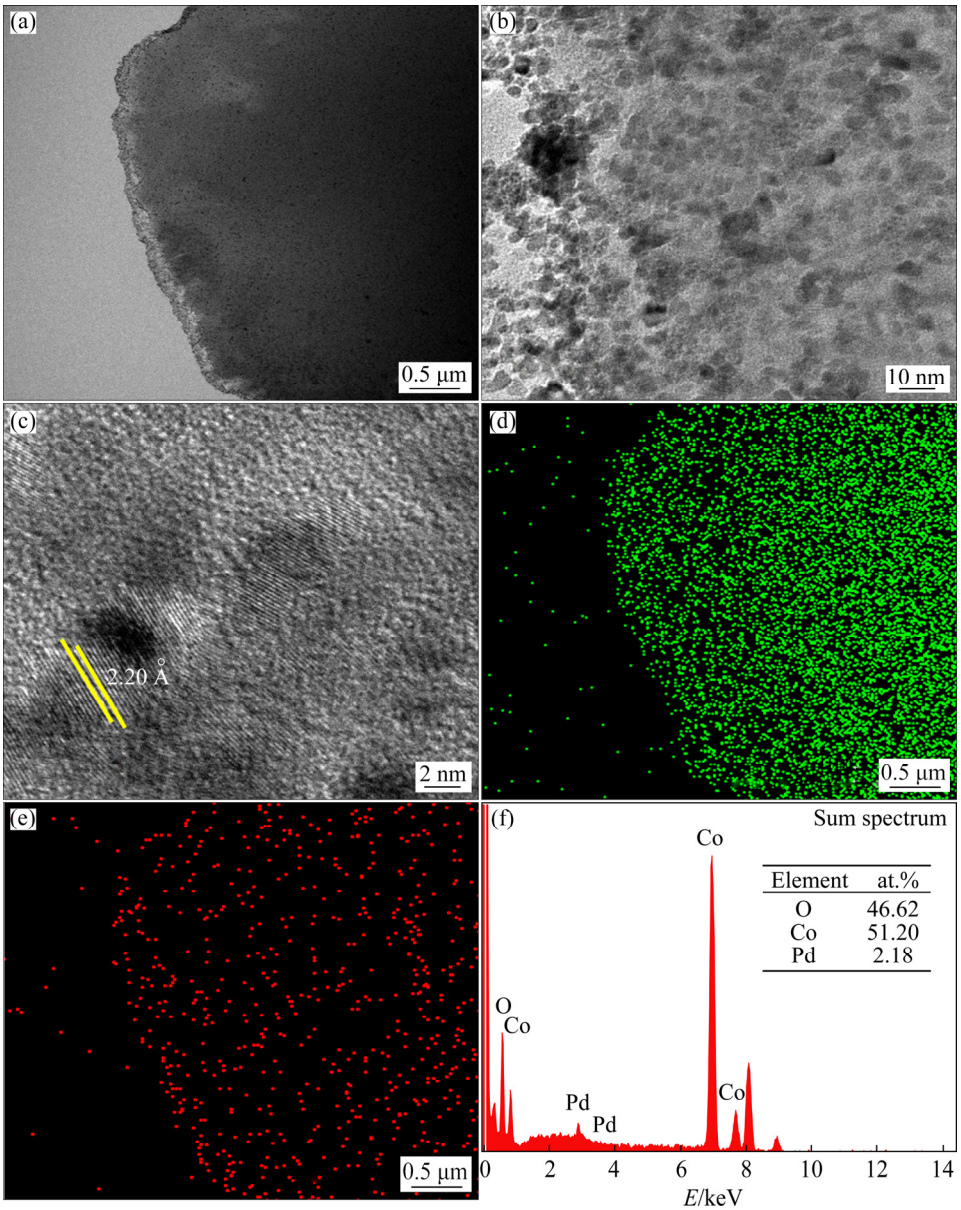

Fig. 3 TEM images (a, b, c), EDS mapping images of Co (d) and Pd (e), and EDS results (f) of $Co(OH)_2$-Pd(1000)

addition, the intensity of the absorption peak at 400 nm is slightly decreased by only 13.4% after 180 min in the absence of the catalyst, which indicates a low reaction rate only in the presence of $NaBH_4$. In the presence of pristine $Co(OH)_2$ nanoplates, the peak intensity is reduced by 27.9% after 180 min, which demonstrates that pristine $Co(OH)_2$ nanoplates exhibit low catalytic activity toward the reduction of 4-NP. According to the previous studies, Co(II) can accelerate the hydrolysis of $NaBH_4$ [33,34]. During $NaBH_4$ hydrolysis, the accelerated electron transfer could promote the reduction of 4-NP. In contrast, $NaBH_4$ hydrolysis could result in $NaBH_4$ deficiency during the catalytic process. Consequently, the complete transformation of 4-NP does not occur. In addition, $NaBH_4$ hydrolysis in the presence of Co(II) could produce cobalt boride compounds, which could greatly reduce the stability of the catalyst, including those of $Co(OH)_2$ and $Co(OH)_2$-Pd. As catalysis occurs in the presence of $Co(OH)_2$-Pd(1000), the intensity of the absorption peak at 400 nm decreases rapidly and the peak disappears within 6 min, as shown in Figs. 5(a) and (b), demonstrating that the prepared $Co(OH)_2$-Pd(1000) exhibits high catalytic activity and can be, thus, applied for the reduction of 4-NP.

To determine the influence of Pd content on the catalytic properties, the performance of $Co(OH)_2$-Pd(500) and $Co(OH)_2$-Pd(1500) for the reduction of

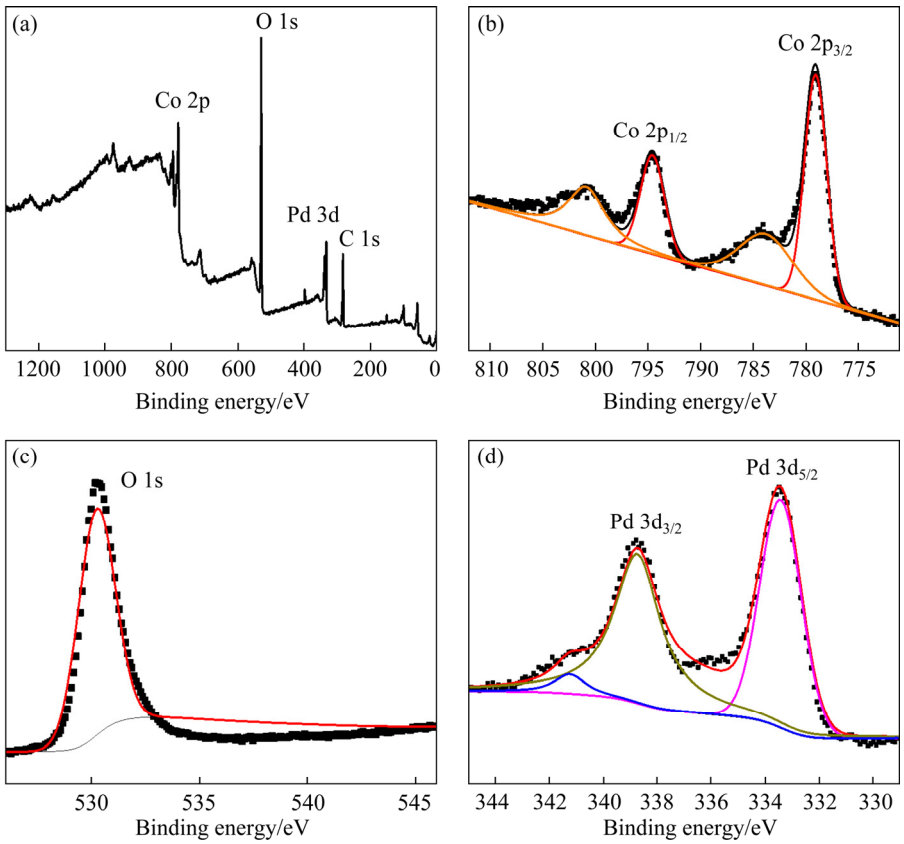

Fig. 4 XPS spectra of $Co(OH)_2$-Pd(1000) nanoplates: (a) Survey scan; (b) Co 2p peak; (c) O 1s peak; (d) Pd 3d peak

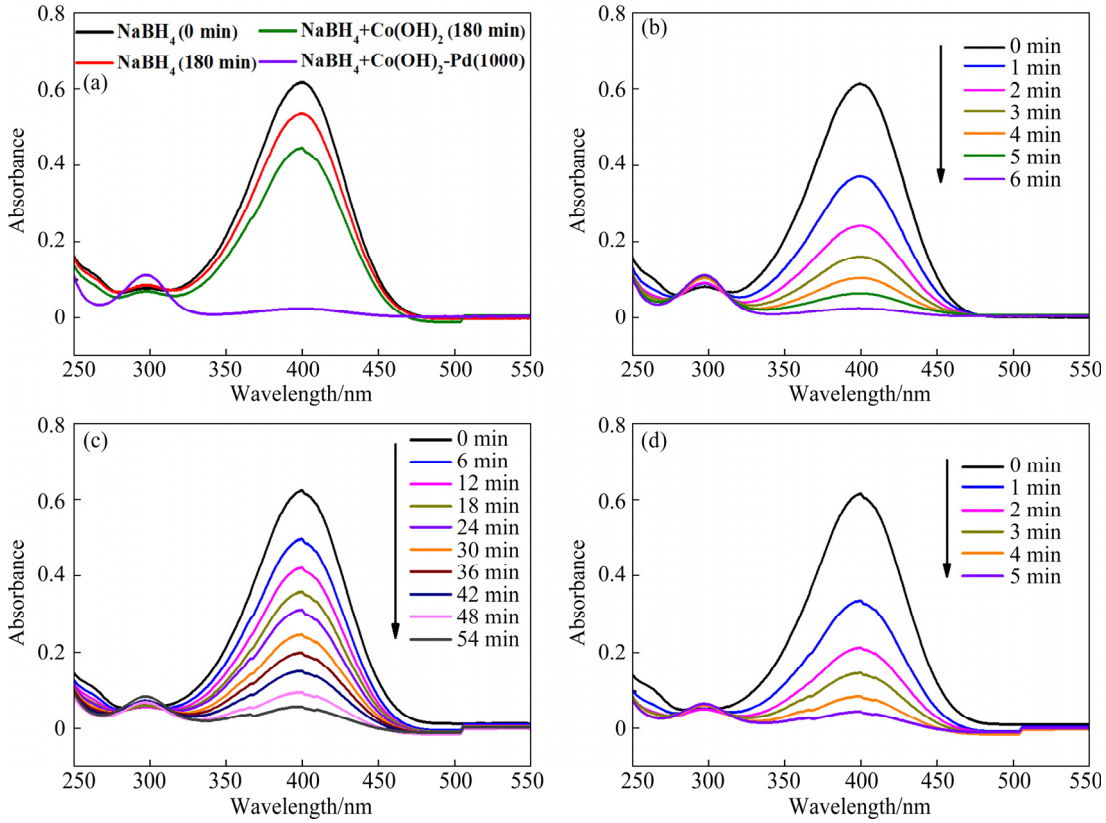

Fig. 5 Catalytic conversion of 4-NP to 4-AP over different catalysts (a), UV-Vis spectra of $Co(OH)_2$-Pd(1000) (b), $Co(OH)_2$-Pd(500) (c), and $Co(OH)_2$-Pd(1500) (d) used for 4-NP reduction

4-NP was also evaluated. As shown in Fig. 5(c), the conversion of 4-NP to 4-AP is completed after 54 min over $Co(OH)_2$-Pd(500), which demonstrates a lower catalytic rate than $Co(OH)_2$-Pd(1000). This may be because $Co(OH)_2$-Pd(500) has a lower Pd content on the $Co(OH)_2$ nanoplates than $Co(OH)_2$-Pd(1000). Furthermore, $Co(OH)_2$-Pd(1500) with a higher Pd content only shows a slightly high catalytic rate, as shown in Fig. 5(d). In the absence of any stabilizer, the Pd nanoparticles probably undergo aggregation during the synthesis process, which eventually affects the performance of $Co(OH)_2$-Pd(1500). Therefore, it is not necessary to further increase the content of Pd on the $Co(OH)_2$-Pd nanoplates. Thus, the $Co(OH)_2$-Pd(1000) nanoplates were used for the next test.

Furthermore, the recyclability of $Co(OH)_2$-Pd(1000) was investigated. After catalysis, the catalyst was separated by sedimentation and used for the next catalytic reaction. The pseudo-first-order kinetic model can be applied to determining the catalytic activity (Fig. 6), which can be defined by

$$\ln A_t = -kt$$

where A_t is the absorbance at 400 nm corresponding to reduction time t, and k is the observed pseudo-first-order rate constant [35]. Table 1 lists the k and square of the correlation coefficient (R^2) values for the first three tests. According to the linear relationship between $\ln A_t$ and t, the rate of constant of this reaction (k) in the first test is ~0.0089 s^{-1}, which indicates that $Co(OH)_2$-Pd(1000) exhibits higher catalytic activity than Pd nanoparticles supported on mesoporous silica (0.004 s^{-1} vs 0.0089 s^{-1}) and its catalytic activity is comparable to that of Pd NPs/CNT-220 (0.0105 s^{-1} vs 0.0089 s^{-1}) [36,37]. In addition, the k value decreases gradually in the second and third catalytic tests, which may be due to the instability of $Co(OH)_2$ in the presence of $NaBH_4$.

Table 1 Parameters of pseudo-first-order kinetic model for catalytic reduction of 4-NP during first three catalytic tests

Cycle	R^2	k/s^{-1}
1	0.9876	0.0089
2	0.9777	0.0051
3	0.9758	0.0041

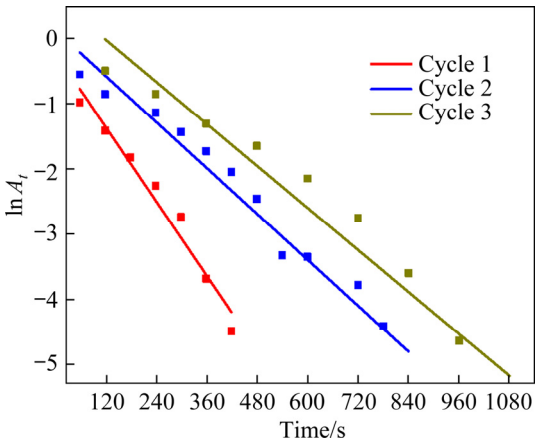

Fig. 6 $\ln A_t$ vs time plot for reduction reaction of 4-NP during first three catalytic tests

4 Conclusions

(1) By using a facile and economical method in the aqueous phase at room temperature, Pd nanoparticles (2−5 nm) are well dispersed on the surface of $Co(OH)_2$ nanoplates in the absence of a stabilizer.

(2) By changing the volume of the precursor (Na_2PdCl_4), the content of Pd on the $Co(OH)_2$ nanoplates could be adjusted. Among the samples, the $Co(OH)_2$-Pd(1000) nanoplates with 2.18 at.% Pd show the capability to complete the conversion of 4-NP in 6 min and can be recycled several times.

(3) The as-prepared $Co(OH)_2$-Pd nanoplates exhibit high catalytic activity toward the reduction of 4-NP and good recyclability. We also believe that the proposed method can be extended to anchor other metals onto $Co(OH)_2$ nanoplates. In addition, the stability of $Co(OH)_2$-Pd(1000) needs to be improved by further research work.

Acknowledgments

The authors are grateful for the financial supports from the National Natural Science Foundation of China (Nos. 51974116, 51874128), and the Science Foundation of Hunan Province, China (Nos. 2020JJ4273, 2020JJ5130).

References

[1] NARAYANAN K B, SAKTHIVEL N. Heterogeneous catalytic reduction of anthropogenic pollutant, 4-nitrophenol by silver-bionanocomposite using cylindrocladium floridanum [J]. Bioresource Technology, 2011, 102: 10737−10740.

[2] XIAO Fa-xin, JIAO Guang-hui, SHEN Hua, LI Kang-bo, OUYANG Yong-zhong, ZHANG Wei-zhe, CHEN Guo-bao, PENG Yu. Influences of pretreatment of carbon on performance of carbon supported Pd nanocatalyst for nitrobenzene hydrogenation [J]. Journal of Nanoscience and Nanotechnology, 2020, 20: 629−635.

[3] FU Si-mei, LI Gang-sen, WEN Xing, FAN Cai-mei, LIU Jian-xin, ZHANG Xiao-chao, LI Rui. Effect of calcination temperature on microstructure and photocatalytic activity of BiOX (X=Cl, Br) [J]. Transactions of Nonferrous Metals Society of China, 2020, 30(3): 765−773.

[4] YANG Bao-jun, LUO Wen, LIAO Qi, ZHU Jian-yu, GAN Min, LIU Xue-duan, QIU Guan-zhou. Photogenerated-hole scavenger for enhancing photocatalytic chalcopyrite bioleaching [J]. Transactions of Nonferrous Metals Society of China, 2020, 30(1): 200−211.

[5] SHAHEEN S M, NIAZI N K, HASSAN N E E, BIBI I, WANG H L, TSANG D C W, OK Y S, BOLAN N, RINKLEBE J. Wood-based biochar for the removal of potentially toxic elements in water and wastewater: A critical review [J]. International Materials Reviews, 2019, 64(4): 216−247.

[6] ZHANG Yu-yuan, HU Hua-wen, CHANG Meng-lei, CHEN Dong-chu, ZHANG Min, WU Liang-peng, LI Xin-jun. Non-uniform doping outperforms uniform doping for enhancing the photocatalytic efficiency of Au-doped TiO_2 nanotubes in organic dye degradation [J]. Ceramics International, 2017, 43(12): 9053−9059.

[7] SHAN Rui, LU Li-li, GU Jing, ZHANG Yu-yuan, YUAN Hao-ran, CHEN Yong, LUO Bo. Photocatalytic degradation of methyl orange by Ag/TiO_2/biochar composite catalysts in aqueous solutions [J]. Materials Science in Semiconductor Processing, 2020, 114: 105088.

[8] JIANG Xue-ding, LAI Shu-feng, XU Wei-cheng, FANG Jian-zhang, CHEN Xin, BEIYUAN Jing-zi, ZHOU Xi-wu, LIN Kai-chun, LIU Jun-xing, GUAN Gong-cou. Novel ternary BiOI/g-C_3N_4/CeO_2 catalysts for enhanced photocatalytic degradation of tetracycline under visible-light radiation via double charge transfer process [J]. Journal of Alloys and Compounds, 2019, 809: 151804.

[9] CHEN Xiao-juan, LI Ning, XU Song, WANG Hai-long, CAI Yu-min. Study on the visible-light photocatalytic performance and degradation mechanism of diclofenac sodium under the system of hetero-structural $CuBi_2O_4$/Ag_3PO_4 with H_2O_2 [J]. Materials, 2018, 11(4): 511.

[10] XU Wen-tao, CHEN Jian-an, QIU Yin, PENG Wei, SHI Ni, ZHOU Ji-cheng. Highly efficient microwave catalytic oxidation degradation of 4-nitrophenol over magnetically separable $NiCo_2O_4$−$Bi_2O_2Co_3$ composite without adding oxidant [J]. Separation and Purification Technology, 2019, 213: 426−436.

[11] CHANG Yang-chuang, CHEN Dong-hwang. Catalytic reduction of 4-nitrophenol by magnetically recoverable Au nanocatalyst [J]. Journal of Hazardous Materials, 2009, 165: 664−669.

[12] WANG Chun, ZHANG Hai-yan, FENG Cheng, GAO Shu-tao, SHANG Ning-zhao, WANG Zhi. Multifunctional Pd@MOF core-shell nanocomposite as highly active catalyst for p-nitrophenol reduction [J]. Catalysis Communications, 2015, 72: 29−32.

[13] LIU Mei-ling, ZHAO Zi-peng, DUAN Xiang-feng, HUANG Yu. Nanoscale structure design for high-performance Pt-based ORR catalysts [J]. Advanced Materials, 2019, 31: e1802234.

[14] KOCZKUR K M, MOURDIKOUDIS S, POLAVARAPU L, SKRABALAK S E. Polyvinylpyrrolidone (PVP) in nanoparticle synthesis [J]. Dalton Transactions, 2015, 44: 17883−17905.

[15] GU Kai, PAN Xue-ting, WANG Wei-wei, MA Jue-jie, SUN Yun, YANG Hai-long, SHEN He-yun, HUANG Zhi-jun, LIU Hui-yu. In situ growth of Pd nanosheets on g-C_3N_4 nanosheets with well-contacted interface and enhanced catalytic performance for 4-nitrophenol reduction [J]. Small, 2018, 14: e1801812.

[16] XIAO Fa-xin, JIAO Guang-hui, LI Kang-bo, ZHANG Wei-zhe, CHEN Guo-bao, DU Jing-jing, PENG Yu. Influences of reducing agents on performance of carbon supported Pd nanocatalyst for hydrogenation of nitrobenzene [J]. Nanoscience and Nanotechnology Letters, 2018, 10(12): 1732−1737.

[17] WANG Deng, LIU Jin, XI Jiang-bo, JIANG Ji-zhou, BAI Zheng-wu. Pd−Fe dual-metal nanoparticles confined in the interface of carbon nanotubes/N-doped carbon for excellent catalytic performance [J]. Applied Surface Science, 2019, 489: 477−484.

[18] XIE Lei, YUAN Kai, XU Jian-xiong, ZHU Yi-rong, XU Li-jian, LI Na, DU Jing-jing. Comparative study on supercapacitive performances of hierarchically nanoporous carbon materials with morphologies from submicrosphere to hexagonal microprism [J]. Frontiers in Chemistry, 2020, 8: 599981.

[19] XU Jian-xiong, DU Guo, XIE Lei, YUAN Kuai, ZHU Yi-rong, XU Li-jian, LI Na, WANG Xian-you. Three-dimensional walnut-like, hierarchically nanoporous carbon microspheres: One-pot synthesis, activation, and supercapacitive performance [J]. ACS Sustainable Chemistry and Engineering, 2020, 8: 8024−8036.

[20] TANG Z M, HAN G H, JUNG E, SEO M G, LEE K Y, KIM W S, YU T. Synthesis of Cu−Pd nanoplates and their catalytic performance for H_2O_2 generation reaction [J]. Molecular Catalysis, 2018, 452: 117−122.

[21] ZHOU A-wu, GUO Rui-mei, ZHOU Jian, DOU Yi-bo, CHEN Ya, LI Jian-rong. Pd@ZIF-67 derived recyclable Pd-based catalysts with hierarchical pores for high-performance heck reaction [J]. ACS Sustainable Chemistry and Engineering, 2018, 6: 2103−2111.

[22] SONG Yan-yan, DUAN Dong, SHI Wen-yu, WANG Hai-yang, SUN Zhan-bo. Facile synthesis of 3D nanoporous Pd/Co_2O_3 composites with enhanced catalytic performance for methanol oxidation [J]. Transactions of Nonferrous Metals Society of China, 2018, 28(4): 676−686.

[23] WANG Jian-cheng, LIU Cong-xue, KAN Xuan, WU Xiao-wei, KAN Jing-lan, DONG Yu-bin. Pd@COF-QA: A phase transfer composite catalyst for aqueous Suzuki−Miyaura coupling reaction [J]. Green Chemistry, 2020, 22: 1150−1155.

[24] LIU Ting, SUN Ying-hui, JIANG Bo, GUO Wei, QIN Wei, XIE Yi-ming, ZHAO Bo, ZHAO Liang, LIANG Zhi-qiang, JIANG Lin. Pd nanoparticle-decorated 3D-printed

hierarchically porous TiO_2 scaffolds for the efficient reduction of a highly concentrated 4-nitrophenol solution [J]. ACS Applied Materials and Interfaces, 2020, 12: 28100−28109.

[25] LONG Yan, LI Jian, WU Lan-lan, LI Jun-qi, WANG Xiao, YAO Shuang, SONG Shu-yan, ZHANG Hong-jie. One-pot synthesis of cobalt−doped Pt−Au alloy nanoparticles supported on ultrathin α-$Co(OH)_2$ nanosheets and their enhanced performance in the reduction of p−nitrophenol [J]. European Journal of Inorganic Chemistry, 2017, 2017(1): 146−152.

[26] XING Zhi-cai, HAN Ce, WANG De-wen, LI Qun, YANG Xiu-rong. Ultrafine Pt nanoparticle-decorated $Co(OH)_2$ nanosheet arrays with enhanced catalytic activity toward hydrogen evolution [J]. ACS Catalysis, 2017, 7: 7131−7135.

[27] YANG Le, WANG Na, TAO Bai-rui, MIAO Feng-juan, ZANG Yu, CHU P K. $Co(OH)_2$ nanosheet arrays electrodeposited with palladium nanoparticles for hydrogen evolution reaction [J]. Journal of Alloys and Compounds, 2019, 810: 151775.

[28] CHEN Li-song, ZHANG Hui-lin, CHEN Li, WEI Xin-fa, SHI Jian-lin, HE Ming-yuan. Facile synthesis of Cu doped cobalt hydroxide (Cu-$Co(OH)_2$) nano-sheets for efficient electrocatalytic oxygen evolution [J]. Journal of Materials Chemistry A, 2017, 5: 22568−22575.

[29] WEN Pu-shan, HUANG Jun-li, KANG Min, CHEN Shu-jun, XU Li-jian, TANG Zeng-min. A facile synthesis of cobalt hydroxide nanoplates and electrochemical performance in supercapacitor application [J]. Materials Express, 2021, 11: 551−556.

[30] DENG Dong-yang, XING Xin-xin, CHEN Nan, LI Yu-xiu, WANG Yu-de. Hydrothermal synthesis of β-$Co(OH)_2$ nanoplatelets: A novel catalyst for CO oxidation [J]. Journal of Physics and Chemistry of Solids, 2017, 100: 107−114.

[31] BAO Lin, LI Tao, CHEN Shu, HE Yi-kuan, PENG Chang, LI Ling, XU Qian, OU En-cai, XU Wei-jian. Electronic-channel in 3D flowery $Co(OH)_2$/N-doped graphene composites with enhanced electrochemistry performance [J]. Materials Letters, 2016, 185: 72−76.

[32] LI Xiang, DONG Fu-ping, ZHANG Li-hua, XU Qin-qin, ZHU Xian-yi, LIANG Song-miao, HU Li-jie, XIE Hai-bo. Cellulosic protic ionic liquids hydrogel: A green and efficient catalyst carrier for Pd nanoparticles in reduction of 4-nitrophenol in water [J]. Chemical Engineering Journal, 2019, 372: 516−525.

[33] LU Jian-ming, DREISINGER D B, COOPER W C. Cobalt precipitation by reduction with sodium borohydride [J]. Hydrometallurgy, 1997, 45: 305−322.

[34] DEMIRCI U B, MIELE P. Cobalt in $NaBH_4$ hydrolysis [J]. Physical Chemistry Chemical Physics, 2010, 12: 14651−14665.

[35] SHAHZAD A, KIM W S, YU T. Synthesis, stabilization, growth behavior, and catalytic activity of highly concentrated silver nanoparticles using a multifunctional polymer in an aqueous-phase [J]. RSC Advances, 2015, 5: 28652−28661.

[36] GU Xian-mo, QI Wei, XU Xian-zhu, SUN Zhen-hua, ZHANG Li-yun, LIU Wei, PAN Xiao-li, SU Dang-sheng. Covalently functionalized carbon nanotube supported Pd nanoparticles for catalytic reduction of 4-nitrophenol [J]. Nanoscale, 2014, 6: 6609−6616.

[37] THOMAS A M, MOHAN A, ROUT L, NAGAPPAN S, PARK S S, HA C S. Pd nanoparticle incorporated mesoporous silicas with excellent catalytic activity and dual responsivity [J]. Colloids and Surfaces A: Physicochemical and Engineering Aspects, 2020, 585: 124074.

无稳定剂水相体系中氢氧化钴纳米片沉积钯用于催化还原 4-硝基苯酚

唐曾民[1]，张 玲[1]，杜晶晶[2]，许利剑[1]

1. 湖南工业大学 生命科学与化学学院 生物医用纳米材料与器件湖南省重点实验室，株洲 412007；
2. 湖南工业大学 包装与材料工程学院，株洲 412007

摘 要：在水溶液中制备负载钯的氢氧化钴($Co(OH)_2$-Pd)纳米片，并将其作为催化剂用于还原 4-硝基苯酚。为了制备 $Co(OH)_2$-Pd 纳米片，Pd 纳米颗粒在室温和没有稳定剂的情况下通过抗坏血酸还原 Na_2PdCl_4 后固定在 $Co(OH)_2$ 纳米片上。透射电镜和扫描电镜观察表明，尺寸为 2~5 nm 的 Pd 纳米颗粒均匀地分散在 $Co(OH)_2$ 纳米片表面。在催化测试中，制备的 2.18% Pd(摩尔分数)沉积的 $Co(OH)_2$-Pd(1000)纳米片可以在 6 min 内催化并完成 4-硝基苯酚向 4-氨基苯酚的转化，第一次测试的动力学常数为 0.0089 s^{-1}。该催化剂经过几个循环后仍保持较高的活性。结果表明，在 $NaBH_4$ 存在下，$Co(OH)_2$-Pd(1000)纳米片对 4-硝基苯酚的还原表现出较高的催化活性。

关键词：Pd 纳米粒子；$Co(OH)_2$ 纳米片；无稳定剂；催化剂；4-硝基苯酚

(Edited by Xiang-qun LI)